

Numerical Model for the Deformation of Nucleated Cells by Optical Stretchers

Ihab Sraj

Division of Physical Sciences and Engineering
King Abdullah University of Science and Technology
Thuwal, Saudi Arabia
ihab.sraj@gmail.com

Joshua Francois

Department of Mechanical Engineering
University of Maryland Baltimore County
Baltimore, Maryland 21250, USA
fjoshua1@umbc.edu

David W.M. Marr

Department of Chemical and Biological Engineering
Colorado School of Mines,
Golden, Colorado 80401, USA
dmarr@mines.edu

Charles D. Eggleton

Department of Mechanical Engineering
University of Maryland Baltimore County
Baltimore, Maryland 21250, USA
eggleton@umbc.edu

Abstract

In this paper, we seek to model the deformation of nucleated cells by single diode-laser bar optical stretchers. We employ a recently developed computational model, the Dynamic Ray-Tracing method, to determine the stress distribution induced by the applied optical forces on a capsule encapsulating a nucleus of different optical properties. These forces are shape dependent and can deform real non-rigid objects; thus resulting in a dynamically changing optical stress distribution with cell and nucleus deformation. Chinese hamster ovary cell is a common biological cell that is of interest to the biomedical community because of their use in recombinant protein therapeutics and is an example of a nucleated cell. To this end, we model chinese hamster ovary cells as two three-dimensional elastic capsules of variable inner capsule size immersed in a fluid where the hydrodynamic forces are calculated using the Immersed Boundary Method. Our results show that the presence of a nucleus has a major effect on the force distribution on the cell surface and the net deformation. Scattering and gradient forces are reported for different nucleus sizes and the effect of nucleus size on the cell deformation is discussed.

1 Introduction

The ability to trap particles using laser light was discovered by Arthur Ashkin in 1970 [1]. In this, gradient forces are created at the surface of transparent particles suspended in a medium of different refractive index and situated within a light gradient. In the ray-optics regime, where the particles size is much larger than the light wavelength [2], refraction of light rays of different intensities at the surface and within the particles results in a change in the total momentum between the entering and exiting light beam. These gradient forces on the order of picoNewtons are capable of drawing microscopic particles into a region of highest light intensity [3]. Scattering forces are also created that accelerate the particle in the direction of beam propagation towards its focus [4]. With these opposing mechanisms, an equilibrium position is reached and the particle is held fixed (trapped) in the center of the beam focus as the light rays passing through and exiting the particle exert forces that are balanced with no net change in momentum.

Optical traps or tweezers used to manipulate microscopic objects without any mechanical contact have become a major tool in biological research over the last thirty years. Cells have been stretched [5], folded [6] and even rotated [6, 7] using single and multiple optical tweezers. Recently, the technique has been extended to study the properties of cells by observing their deformation [8, 9, 10]. Guck *et al.* developed an optical stretcher that uses two counterpropagating diverging laser beams to trap cells individually along the aligned laser beams axis [5]. This optical stretcher has also been used to deform cells and to measure their membrane properties using a simple numerical model [9]. Extending this, Sraj *et al.* developed a high-throughput optical stretcher using a single linear diode bar to trap and stretch bovine red blood cells (RBC) [10].

Theoretical and numerical studies have also been conducted to determine the induced optical force distribution. Using analytical solutions of the governing optical equations, Ashkin was the first to perform calculation of the total forces of a single-beam gradient laser on solid spheres in the ray-optics (RO) regime [11]. Guck *et al.* determined the local optical force distribution by the dual optical stretcher on spherical cells using the RO technique before cells begin to deform [5] to determine the stiffness of RBCs [9]. In their method, the effect of subsequent deformation on the calculation of force distribution was neglected and constant rigid spherical cell morphology was assumed due to limitations in the method. Deformability of biological cells can result in a shape change under the influence of external flows or applied forces and thus the local force distribution and total trapping forces can change significantly with cell deformation [12]. To take this into account, the RO method has been improved to include different cell shapes such as oblate spheroids [13] and even cylinders [14]. As an analytical method, RO remains a difficult approach for calculating the forces on more complex cell shapes like the RBC bi-concave discoid shape and deformable cells.

To overcome these issues, we recently developed and implemented a dynamic ray-tracing (DRT) approach [12] that, in addition to finding transient optical

forces on deformable cells, solves for fluid-cell interactions [15, 16]. DRT offers the possibility of simulating different phenomena occurring in optical systems such as erythrocyte deformation in high-throughput optical stretchers [17] and optical levitation [18]. The approach allows one to assess cell deformability and to investigate the optical parameters to better design traps and manipulate cells prior to performing experiments. In addition, due the vector-based nature, DRT allows the calculations of both anisotropic and inhomogeneous structures, cases that exist in real systems.

CHO cells are the most commonly used mammalian host for industrial production of recombinant protein therapeutics [19] and have been used in related genetics studies [20]. Because of their importance, a number of previous studies have investigated the optical forces on CHO cells. For example, Wei *et al.* used a fiber-optic dual-beam trap to capture chinese hamster ovary (CHO) cells and determine the associated three-dimensional optical force field [21]. Chang *et al.* developed a model based on RO to calculate the optical force upon a solid spherically-symmetric multilayer sphere [22]. This study showed that the magnitude of optical forces are three times smaller than that upon a polystyrene bead of the same size and that the distribution of optical forces is much different from that upon a uniform particle. Recently, Kim *et al.* computed the optical force on a pair of concentric spheres in a focused beam and determined the influence of refractive index differences and relative size between the inner and outer spheres on the optical force [23].

All of these studies however did not take into account the deformability of both the cell and its encapsulated nucleus. We show here how the presence of a nucleus inside deformable cells leads to alteration in the propagation of light rays due to the additional internal surface and the additional medium of different refractive index [24]. Here, the variation in the nucleus size may significantly influence the optical forces and ultimately the net deformation of both the cell and the nucleus itself.

2 Numerical method

Simulating deformation of a cell via optical stretchers requires a two-step method to first determine optical stresses induced by the interaction of light with the cell surface and then model the cell-fluid interactions. Because the distribution of optical stresses is dependant on the shape of the cell that in turn changes during deformation, these two steps are done alternately until a steady state shape is reached. In the case of nucleated cells, optical stress calculation is additionally challenging due to the different external and internal morphologies in addition to membrane deformability. For this purpose, we resort to DRT to determine the optical stresses induced on the surfaces of deformable nucleated cells by optical stretchers [10, 17]. DRT, unlike the traditional RO method, is vector-based and is capable of determining the optical forces on cells of arbitrary shape and morphology. Cell-fluid interaction and the hydrodynamics, on the other hand, are solved using the Immersed Boundary Method (IBM). In this

section we briefly describe the two methods.

2.1 Dynamic Ray Tracing

DRT is a vector-based method developed by Sraj *et al.* [12, 17] to determine optical forces on the surface of any arbitrary shaped cell including deformable cells with asymmetrical geometries [18]. Briefly, DRT considers a finite number of rays issued from a light source with given intensities and known direction. These rays are treated as vectors and traced as they intersect a surface. A ray-triangle intersection algorithm is then employed to determine the location of intersection where the surface is divided into triangular elements for this purpose. Geometrical optics laws are then applied to find the refraction and reflection angle. Consequently the vectors of the rays are updated and the procedure is repeated till each ray exits the cell. From the direction of the light rays within the cell one can calculate the trapping efficiency Q , a dimensionless factor representing the amount of momentum transferred [5, 12]. The trapping efficiency Q is independent of the laser power used and depends only on the object geometry and reflectance of the medium. Elemental optical forces at any location of the cell are therefore found regardless of the initial cell shape. Rays are traced at any surface where Q is multiplied by a factor to account for energy loss from previous refractions. Internal and external reflections within the cell are neglected as their effects rapidly diminish. Optical forces can be expressed as

$$F_{optical} = \frac{n_m Q P}{c}, \quad (1)$$

where n_m is the index of refraction of the buffer medium, c the speed of light in vacuum, and P the laser power. It is important to note that the resulting optical forces are added to the Navier-Stokes equations as body forces as described below.

This method has been validated and applied to cells of different initial shapes [12] and different optical applications [17, 18]. Here, DRT is used to model nucleated cells by considering two concentric spheres of different sizes, one representing the cell surface and another representing the nucleus. DRT is then employed to determine optical stresses induced on both surfaces.

2.2 Immersed Boundary Method

The IBM is a cell-fluid interaction solver that has been used extensively to simulate biological systems such as cell adhesion [25], cell adhesion in atomic force microscopy measurements [26] and red blood cell motion through microvascular bifurcation [27]. IBM splits the numerical solution onto two grids: a stationary grid that has a fixed position with time representing the three-dimensional fluid domain and a moving grid representing the two-dimensional immersed boundary.

To this end, a cell is modeled as an elastic membrane that is deformable by any applied stress. The membrane is discretized into a finite number of flat triangular elements that remain flat after deformation. This approximation is valid given that the local radius of curvature during deformation is much larger than the membrane thickness and that bending stresses are negligible. Elastic forces at the discrete membrane nodes are found from their displacement (deformation) using a finite element model. We adopt an approach developed by Charrier *et al.* [28] and Shrivastava and Tang [29] that uses the principle of virtual work to find those forces from an appropriate strain energy density function. These forces and any external applied forces such as the optical forces are then distributed onto the fluid grid using an appropriate discrete delta function and added to the Navier-Stokes equations as body forces. The discrete delta function ensures that only membrane nodes in the sphere of influence of the fluid grid make a contribution to the local body forces. The Navier-Stokes equations are then solved for the fluid velocity.

The no-slip boundary condition at the membrane surface is satisfied by allowing the membrane nodes to move with the local fluid velocity. The velocity of the membrane is found by summing of the velocities at the fluid grid nodes weighted by the same discrete delta function used for the distribution of body forces. This again ensures that only fluid grid nodes in the sphere of influence of the membrane node make a contribution to its velocity. Membrane nodes are then moved with the calculated velocity for one time step to a new position giving a new membrane shape. The procedure is repeated and elastic forces and optical forces are then calculated as described above to advance the flow for another time step.

3 Model parameters

The CHO cell is a typical example of a nucleated cell. The size of such cells vary with radius r_{cell} ranging from $5 - 7.5 \mu m$ [30] and nucleus radius r_{nuc} varying following the relationship [31]:

$$r_{cell} = (1.38 \pm 0.02)r_{nuc} + (0.03 \pm 0.05). \quad (2)$$

The refractive index of the cytoplasm has been measured and reported as $n_{cyt} = 1.37$ while that of the nucleus has been found to be slightly greater $n_{nuc} = 1.392$ [31]. As the size of the cell has an effect on the forces induced by optical stretchers (more surface area intuitively results in large forces) and hence on the cell deformation, we seek to investigate the impact of the presence of the nucleus and its size on the optical stress distribution and resulting cellular deformation. For this purpose, we model CHO cells as two three-dimensional (3D) concentric elastic spherical capsules. The radius of the outer capsule is fixed and taken as the CHO cell average radius $r_{cell} = 5.6 \mu m$; however, the radius of the inner capsule representing the nucleus is varied from $r_{nuc} = 1.1 - 5 \mu m$. The ratio of the radius of the cell to the radius of the nucleus is denoted by $r = \frac{r_{nuc}}{r_{cell}}$. We note that a typical CHO cell has radii ratio of $r = 0.72$ from Equation 2.

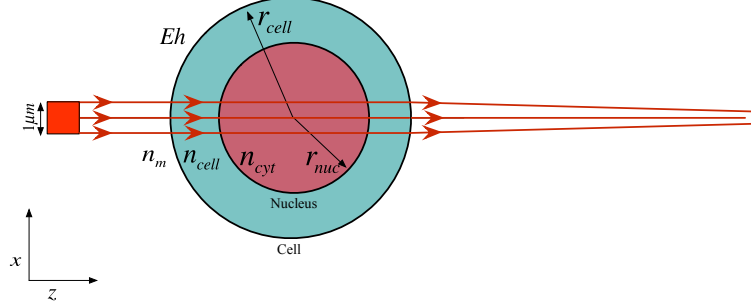


Figure 1: CHO cell model: $n_m < n_{cell} < n_{cyt}$ in a linear diode stretcher.

In our calculations, cells are assumed initially trapped and situated at the center of a laser beam created with a single linear diode bar of wavelength $\lambda = 808 \text{ nm}$ and power $P = 12.5 \text{ mW}/\mu\text{m}$. The length of the diode lies in the y -axis and the laser beam direction is along the z -axis as shown in Fig. 1. The cell is assumed to be immersed in an aqueous medium of refractive index $n_m = 1.335$ that is lower than the refractive index of both the cell and its nucleus ($n_m < n_{cyt} < n_{nuc}$) (Fig. 1).

The hydrodynamics and cell mechanics are calculated using the IBM. Both fluids inside and outside the cell are assumed incompressible and Newtonian with identical density $\rho = 1 \text{ g/cm}^3$ and viscosity $\mu = 0.8 \text{ cP}$. The cell membrane is assumed of Neo-Hookean material, as appropriate for most biological cells, and can be characterized using solely its stiffness Eh . Unless otherwise noted, membrane stiffness is taken as $Eh = 0.1 \text{ dyn/cm}$. For the purpose of quantifying cell deformation from optical or hydrodynamic forces, we use the Taylor deformation parameter defined as: $DF = (L - B)/(L + B)$, where L and B are the major and minor semi-axis of a capsule in the $x - z$ plane. When viscous stresses, elastic forces and optical forces are balanced, cells adopt a steady state shape denoted by DF_∞ . The uniform grid used for the fluid solver has 64^3 nodes with a grid spacing of $r_{cell}/8$ while the finite element cell grid has 20482 triangular elements. A time step of 10^{-5} s was used in all computations to ensure numerical stability.

4 Results and discussions

4.1 Impact of nucleus size on optical forces

As a first step, we investigate the effect of nucleus size on the optical forces initially induced at the cell surface. For reference, we employ DRT to determine the forces induced on a cell with no nucleus. In this case, light rays emerging from the diode laser bar hit the front surface of the cell to create optical scattering forces along the laser beam axis whose direction is opposite to their propagation direction i.e. the negative z -axis direction as shown in Fig. 1.

This is due to the momentum gained by the cell when the rays transit from a medium of lower refractive index to a medium of higher refractive index (the cell cytoplasm $n_{cyt} = 1.37$) [5]. Gradient optical forces are also created with a sum equal to zero as the center of the cell is aligned with the center of the laser beam. After refraction, the rays continue to hit the back surface of the cell where they refract again and transfer momentum inducing scattering forces in the positive direction. The magnitude of the net scattering force at the back surface of the cell is, however, greater than the net scattering force at the front surface resulting in a net total scattering force in the positive z -axis direction. With our chosen laser, cell, and fluid properties, the magnitude of scattering force applied on the front surface is 23.1 pN while on the back surface is 26.7 pN with a net scattering force of 3.6 pN . The scattering forces would both stretch and translate the cell away from the light source. The net gradient forces are again equal to zero on both the front and back surface of the cell; however, if we consider the net gradient force in the perpendicular direction to the laser beam on one half of the cell we find it equal to 20.7 pN . The gradient forces contribute to the stretching of the cell as well but have no translation effect.

In cells with a nucleus, light rays can hit up to four surfaces as shown in Fig. 1 before exiting the cell from the back surface. This leads to scattering and gradient optical forces at both the outer cell and the nucleus surface. At the front cell surface, scattering forces remain unchanged and independent of the nucleus size as the rays first enter the cell as already described. As the refractive index of the nucleus is higher than that of the cytoplasm, scattering forces at the front surface are also in the negative direction while the same forces at the back surface are in the positive direction. However, the magnitude of the net scattering force on the nucleus is less than the net scattering force on the cell due to the smaller refractive index contrast between the nucleus and the cell compared with the cell and suspending medium ($\frac{n_{nuc}}{n_{cyt}} = \frac{1.392}{1.37} = 1.016$ versus $\frac{n_{cyt}}{n_m} = \frac{1.37}{1.335} = 1.030$). The magnitude of these forces depends on the nucleus size. For instance, a nucleus of radius $r_{nuc} = 4 \text{ }\mu\text{m}$ experiences a scattering force of 4.54 pN on the front surface of the nucleus and a force of 5.24 pN on the back surface with a net scattering force on the nucleus of 0.7 pN . When the nucleus size is increased to $r_{nuc} = 5 \text{ }\mu\text{m}$, the net force on the nucleus increases to 8.75 pN and 10.4 pN on the front and back surface respectively with a total net force of 1.6 pN . This increase in force has a significant effect on the nucleus deformation and the forces induced on the cell itself as discussed in the following section.

As the rays reach the cell back surface, the forces induced are influenced by the previous two refractions at the nucleus. As the nucleus size increases, optical forces on the nucleus increase, rays gain more energy, and we see subsequent increase in the magnitude of optical forces at the back cell surface. For a nucleus of radius $r_{nuc} = 4 \text{ }\mu\text{m}$ the net force at the back of the cell is 27.1 pN and 27.4 pN for $r_{nuc} = 5 \text{ }\mu\text{m}$. The maximum increase in the net optical forces on the cell is thus 20.4% compared with the nucleus-free case. Finally, for $r_{nuc} = 5 \text{ }\mu\text{m}$ the gradient forces calculated on the cell slightly decreased to 20.2 pN due to

the presence of the nucleus while the gradient forces calculated on the nucleus increased to 8.6 pN .

The variation of the net scattering and gradient forces on the cell and its nucleus is shown in Fig. 2 where we clearly see the effect of the size of the nucleus on the total net force induced on the cell surface. As the nucleus size increases, the cell will be exposed to larger forces for the same laser power. The nucleus acts as a lens that focuses the light rays and leads to higher optical forces at the nucleus and cell back surfaces. We finally note that we can determine the net scattering and gradient forces on a CHO cell of nominal size from the curves in Fig. 2 using a vertical line (shown in magenta) that corresponds to the nominal CHO cell radius ratio of $r = 0.72$.

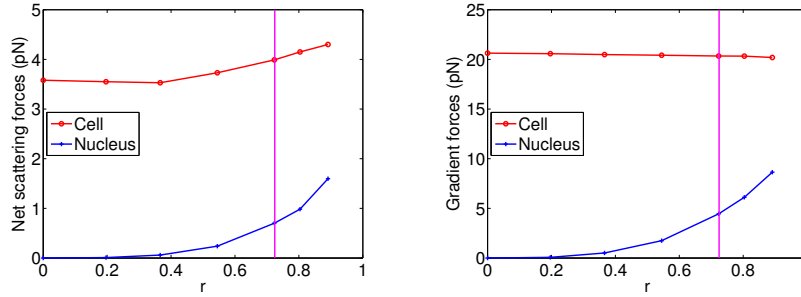


Figure 2: Comparison of the magnitude of optical forces on a CHO cell for different nucleus radii: (left) net scattering forces (right) gradient forces. The vertical line in magenta corresponds to the nominal CHO cell radius ratio of $r = 0.72$.

4.2 Influence of nucleus size on net cell deformation

From our calculations, it is clear that the presence of a nucleus has a significant impact on the initial optical force distribution as these forces deform and stretch CHO cells. Changes in cell shape lead to a new force distribution. To calculate these, optical forces are added as body forces to the surrounding fluid. DRT is then employed to update the optical force distribution as the cell shape is changing until steady state when the elastic and applied optical forces are equal.

The net deformation of both the cell and the nucleus is quantified using the Taylor parameter deformation DF shown in Fig. 3. The figure indicates that in the case of small nuclei, DF of the cell increases to a steady value that is higher than the reference case of no-nucleus (shown on all panels for comparison). This is due to the slight decrease in gradient forces that lead to more deformation in the z -direction and thus higher net deformation. DF of the nucleus, however, is negligible due to the small magnitudes of the optical forces created.

For larger nuclei, DF shows similar trends where the cell deforms until a steady state shape is reached but with net deformation lower than the nucleus-

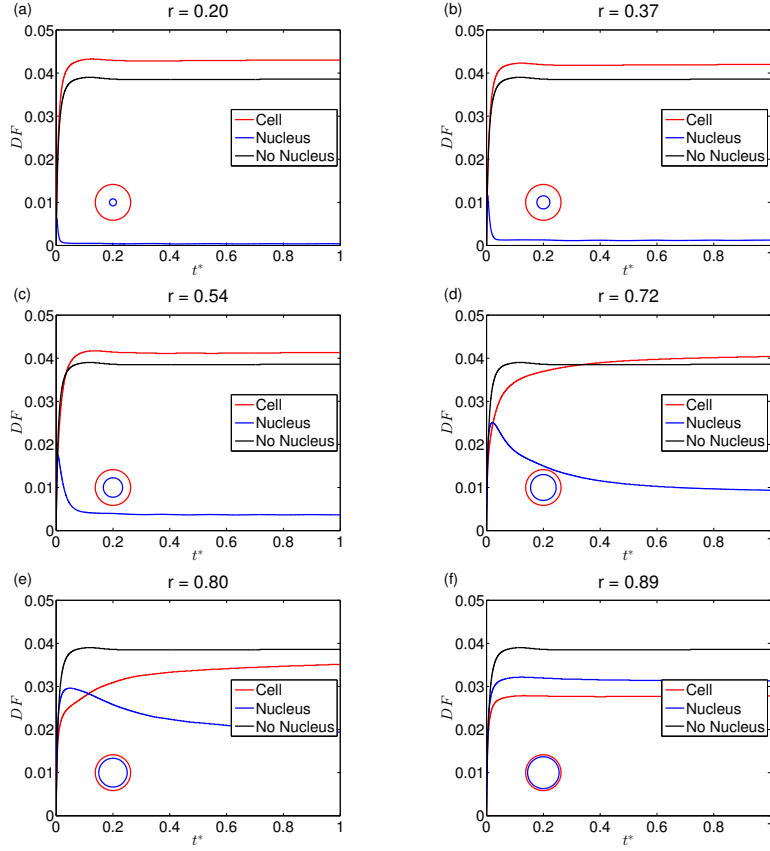


Figure 3: Evolution of net deformation DF (of both a CHO cell and its nucleus) for different nucleus size as indicated. Evolution of net deformation of cell with no-nucleus is also shown for reference.

free case. In this, we see that the net deformation of the cell decreases and the net deformation of the nucleus increases with r .

To summarize the results discussed above, we show in Fig. 4 the steady state net deformation DF_∞ of both the cell and the nucleus. Here, we clearly see that DF_∞ of the cell is initially larger than the DF_∞ of the nucleus-free case but then decreases as the radius ratio increases. At the same time, DF_∞ of the nucleus increases with the radius ratio. The two curves eventually intersect when the radius of the nucleus becomes comparable to the radius of the cell. We also note here that we can determine the steady state net deformation DF_∞ of a CHO cell of nominal size from the curves in Fig. 4 using a vertical line (shown in magenta) that corresponds to the nominal CHO cell radius ratio of $r = 0.72$.

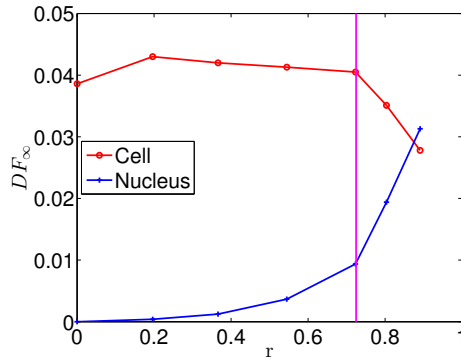


Figure 4: Comparison of net deformation of a CHO cell and its nucleus for different nucleus radii. The vertical line in magenta corresponds to the nominal CHO cell radius ratio of $r = 0.72$.

DF calculations for CHO cells show a clear relationship between the size of the nucleus and the steady state net cell and nucleus deformation. As the size of the nucleus increases, the steady state deformation increases due to the increase in the scattering forces applied at the cell surface. It is therefore expected that the corresponding deformation increases as well. Fig. 4 shows also that as the size of the nucleus increases, the steady state deformation of the cell decreases. Moreover, as the size of the nucleus approaches the size of the cell, the relative deformation of the nucleus, as characterized by the Taylor deformation parameter surpasses that of the cell. The relationship between the size of the nucleus and the deformation of the cell means that cells with larger nuclei show less deformation when optically stretched than cells with smaller nuclei. Another observation is that the cell with no nucleus deformed to a steady state of DF value that is smaller than the value for the smallest radius ratio but larger than the value for the largest radius ratio.

5 Conclusions

Chinese hamster ovary cell is of interest to the biomedical community because of their use in recombinant protein therapeutics. Unfortunately, no experiments have been performed to stretch this line of cells in optical traps. Few experiments, however, were performed to describe deformation of cell nucleus. In these experiments researchers have studied the interaction of cells with topographically patterned material surfaces to show the changes in shape, function, and viability of the cells. Only few of these studies, however, indicated possible impact on the behavior of organelles. For instance, Dalby *et al.* [32] quantified cell and nuclear morphology with light and fluorescence microscopy and showed a slight elongation of the nuclei in grooves. Yamauchi *et al.* also observed the deformation of cancerous cells/nucleus and their migration in capillaries of mince [33]. This study aimed to find the minimum diameter of capillaries where cancer cells are able to migrate. They measured the diameter of both the cell and its nucleus for this purpose.

In our work, we modeled the deformation of Chinese hamster ovary cells by single diode-laser bar optical stretchers. For this purpose, we extended the recently developed Dynamic Ray-Tracing method to determine the stress distribution induced by the applied optical forces on cells that have a nucleus. Our results showed that the presence of a nucleus has a major effect on the force distribution on the cell surface and the net deformation. We also showed and quantified the effect of nucleus size on the net applied force as well as on cell deformation. We are working effectively on setting up experiments to stretch CHO cells and compare our numerical data with experimental results.

6 Acknowledgments

The authors would like to acknowledge financial support provided by the National Institute of Health grant R01 AI079347-04. This work used the Extreme Science and Engineering Discovery Environment (XSEDE), which is supported by National Science Foundation grant number OCI-1053575.

References

- [1] A. Ashkin, “Acceleration and trapping of particles by radiation pressure,” *Phys. Rev. Lett.* **24**, 156–159 (1970).
- [2] H. C. Van De Hulst, *Light Scattering by Small Particles (Structure of Matter Series.)* (Dover Pubn Inc).
- [3] A. Ashkin, J. M. Dziedzic, J. E. Bjorkholm, and S. Chu, “Observation of a single-beam gradient force optical trap for dielectric particles,” *Opt. Lett.* **11**, 288–290 (1986).

- [4] A. Ashkin and J. M. Dziedzic, “Optical levitation by radiation pressure,” *Applied Physics Letters* **19**, 283–285 (1971).
- [5] J. Guck, R. Ananthakrishnan, H. Mahmood, T. J. Moon, C. C. Cunningham, and J. Käs, “The optical stretcher: A novel laser tool to micromanipulate cells,” *Biophysical Journal* **81**, 767 – 784 (2001).
- [6] M. Gu, S. Kuriakose, and X. Gan, “A single beam near-field laser trap for optical stretching, folding and rotation of erythrocytes,” *Opt. Express* **15**, 1369–1375 (2007).
- [7] S. K. Mohanty, A. Uppal, and P. K. Gupta, “Self-rotation of red blood cells in optical tweezers: Prospects for high throughput malaria diagnosis,” *Biotechnology Letters* **26**, 971–974 (2004). 10.1023/B:BILE.0000030041.94322.71.
- [8] P. Bronkhorst, G. Streekstra, J. Grimbergen, E. Nijhof, J. Sixma, and G. Brakenhoff, “A new method to study shape recovery of red blood cells using multiple optical trapping,” *Biophysical Journal* **69**, 1666 – 1673 (1995).
- [9] J. Guck, S. Schinkinger, B. Lincoln, F. Wottawah, S. Ebert, M. Romeyke, D. Lenz, H. M. Erickson, R. Ananthakrishnan, D. Mitchell, and J. K. “Optical deformability as an inherent cell marker for testing malignant transformation and metastatic competence,” *Biophysical Journal* **88**, 3689–3698 (2005).
- [10] I. Sraj, C. D. Eggleton, R. Jimenez, E. Hoover, J. Squier, J. Chichester, and D. W. M. Marr, “Cell deformation cytometry using diode-bar optical stretchers,” *Journal of Biomedical Optics* **15**, 047010 (2010).
- [11] A. Ashkin, “Forces of a single-beam gradient laser trap on a dielectric sphere in the ray optics regime,” *Biophysical Journal* **61**, 569–582 (1992).
- [12] I. Sraj, A. C. Szatmary, D. W. M. Marr, and C. D. Eggleton, “Dynamic ray tracing for modeling optical cell manipulation,” *Opt. Express* **18**, 16702–16714 (2010).
- [13] H. Sosa-Martínez and J. C. Gutiérrez-Vega, “Optical forces on a mie spheroidal particle arbitrarily oriented in a counterpropagating trap,” *J. Opt. Soc. Am. B* **26**, 2109–2116 (2009).
- [14] R. C. Gauthier, “Theoretical investigation of the optical trapping force and torque on cylindrical micro-objects,” *J. Opt. Soc. Am. B* **14**, 3323–3333 (1997).
- [15] C. S. Peskin and D. M. McQueen, “A three-dimensional computational method for blood flow in the heart i. immersed elastic fibers in a viscous incompressible fluid,” *Journal of Computational Physics* **81**, 372 – 405 (1989).

- [16] C. D. Eggleton and A. S. Popel, “Large deformation of red blood cell ghosts in a simple shear flow,” *Physics of Fluids* **10**, 1834–1845 (1998).
- [17] I. Sraj, A. C. Szatmary, S. A. Desai, D. W. M. Marr, and C. D. Eggleton, “Erythrocyte deformation in high-throughput optical stretchers,” *Phys. Rev. E* **85**, 041923 (2012).
- [18] C. B. Chang, W.-X. Huang, K. H. Lee, and H. J. Sung, “Optical levitation of a non-spherical particle in a loosely focused gaussian beam,” *Opt. Express* **20**, 24068–24084 (2012).
- [19] K. P. Jayapal, K. F. Wlaschin, W.-S. Hu, and M. G. S. Yap, “Recombinant Protein Therapeutics from CHO Cells - 20 Years and Counting,” *CHO Consortium: SBE Special Edition* pp. 40–47 (2007).
- [20] J. H. Tjio and T. T. Puck, “Genetics of somatic mammalian cells: Ii. chromosomal constitution of cells in tissue culture,” *The Journal of Experimental Medicine* **108**, 259–268 (1958).
- [21] M.-T. Wei, K.-T. Yang, A. Karmenyan, and A. Chiou, “Three-dimensional optical force field on a chinese hamster ovary cell in a fiber-optical dual-beam trap,” *Opt. Express* **14**, 3056–3064 (2006).
- [22] Y.-R. Chang, L. Hsu, and S. Chi, “Optical trapping of a spherically symmetric sphere in the ray-optics regime: a model for optical tweezers upon cells,” *Appl. Opt.* **45**, 3885–3892 (2006).
- [23] S. B. Kim, K. H. Lee, S. S. Kim, and H. J. Sung, “Optical force on a pair of concentric spheres in a focused laser beam: ray-optics regime,” *J. Opt. Soc. Am. B* **29**, 2531–2541 (2012).
- [24] R. Meyer and A. Brunsting, “Light scattering from nucleated biological cells,” *Biophysical Journal* **15**, 191 – 203 (1975).
- [25] V. Gupta, I. Sraj, K. Konstantopoulos, and C. Eggleton, “Multi-scale simulation of l-selectin-psgl-1-dependent homotypic leukocyte binding and rupture,” *Biomechanics and Modeling in Mechanobiology* **9**, 613–627 (2010). 10.1007/s10237-010-0201-2.
- [26] I. Sraj, K. Y. Chan, K. Konstantopoulos, and C. D. Eggleton, “A numerical study of the influence of cellular adhesion on prestress in atomic force microscopy measurements,” *Journal of Advanced Microscopy Research* **6**, 89–96 (May).
- [27] W. Xiong and J. Zhang, “Two-dimensional lattice Boltzmann study of red blood cell motion through microvascular bifurcation: cell deformability and suspending viscosity effects,” *Biomechanics and Modeling in Mechanobiology* **11**, 575–583 (2012). 10.1007/s10237-011-0334-y.

- [28] J. M. Charrier, S. Shrivastava, and R. Wu, “Free and constrained inflation of elastic membranes in relation to thermoforming non-axisymmetric problems,” *The Journal of Strain Analysis for Engineering Design* **24**, 55–74 (1989).
- [29] S. Shrivastava and J. Tang, “Large deformation finite element analysis of non-linear viscoelastic membranes with reference to thermoforming,” *The Journal of Strain Analysis for Engineering Design* **28**, 31–51 (1993).
- [30] Y. Han, X.-M. Liu, H. Liu, S.-C. Li, B.-C. Wu, L.-L. Ye, Q.-W. Wang, and Z.-L. Chen, “Cultivation of recombinant chinese hamster ovary cells grown as suspended aggregates in stirred vessels,” *Journal of Bioscience and Bioengineering* **102**, 430 – 435 (2006).
- [31] A. Brunsting and P. F. Mullaney, “Differential light scattering from spherical mammalian cells,” *Biophysical Journal* **14**, 439 – 453 (1974).
- [32] M. J. Dalby, M. O. Riehle, S. J. Yarwood, C. D. Wilkinson, and A. S. Curtis, “Nucleus alignment and cell signaling in fibroblasts: response to a micro-grooved topography,” *Experimental Cell Research* **284**, 272 – 280 (2003).
- [33] K. Yamauchi, M. Yang, P. Jiang, N. Yamamoto, M. Xu, Y. Amoh, K. Tsuji, M. Bouvet, H. Tsuchiya, K. Tomita, A. Moossa, and R. M. Hoffman, “Real-time in vivo dual-color imaging of intracapillary cancer cell and nucleus deformation and migration,” *Cancer Research* **65**, 4246–4252 (2005).